Article

Variation Characteristics of Temperature and Rainfall and Their Relationship with Geographical Factors in the Qinling Mountains

Yangna Lei [1,2], Rongwei Liao [3,*], Yumeng Su [4], Xia Zhang [1,2], Duanyang Liu [5,*] and Lei Zhang [6]

1 Shaanxi Climate Center, Xi'an 710014, China
2 Key Laboratory of Eco-Environment and Meteorology for the Qinling Mountains and Loess Plateau, Shaanxi Meteorological Bureau, Xi'an 710014, China
3 State Key Laboratory of Severe Weather, Chinese Academy of Meteorological Sciences, Beijing 100081, China
4 Liaoning Meteorological Bureau, Shenyang 110001, China
5 Key Laboratory of Transportation Meteorology of China Meteorological Administration, Nanjing Joint Institute for Atmospheric Sciences, Nanjing 210041, China
6 Tianjin Meteorological Information Centre, Tianjin 300074, China
* Correspondence: liaorw@cma.gov.cn (R.L.); liuduanyang@cma.cn (D.L.)

Abstract: The Qinling Mountains (QMs) are considered to be the division in geology, geochemistry, and physical geography between northern China and southern China. They have crucial effects on regional climate, especially on rainfall and temperature, and have shown great scientific relevance to climate change research in China. Using the observational daily and monthly rainfall and temperature data derived from meteorological and regional automatic stations—as well as the methods of correlation analysis, climate trend analysis, and Mann–Kendal and *t* tests—we revealed the spatiotemporal change characteristics of temperature and rainfall and their correlation with elevation, longitude, and latitude. The results show that the annual mean temperature (AMT) underwent a significant increasing trend in the QMs. The maximum AMT increase occurred in spring, and the minimum occurred in summer. Positive anomalies of annual mean rainfall amount (AMRA) occurred in the 1960s, 1980s, and 2010s, and negative anomalies occurred in the 1970s, 1990s, and 2000s. In the QMs, the amount of moderate rainfall (MR) occupied the maximum proportion and accounted for 27.9% of the AMRA, whereas the torrential rainfall (TR) occupied the minimum proportion and accounted for 12.8%. The AMRA amount significantly decreased by 130.1 mm from the 1980s to the 1990s and accounted for 13.5% of the measure in the 1980s. The AMT and AMRA showed consistent change trends with increases in elevation and latitude and showed the opposite trend as the longitude increased. The results offer a further understanding of the meteorological background of the QMs, helping us in further investigating the potential physical mechanisms that influence the spatiotemporal distribution characteristics of temperature and rainfall in the QMs. This study will provide a scientific basis for rainfall and temperature forecasts, with relevance to local ecosystems, agriculture, soil erosion, and the prevention and mitigation of floods in the future.

Keywords: Qinling mountains; temperature; rainfall; change characteristics; geographical factors

1. Introduction

Global warming has increased the scope of climate system changes, leading to frequent extreme rainfall events, high temperature events, and drought events, which seriously threaten the safety of global ecological and environmental systems [1–4]. According to the *Sixth Assessment Report* of the Intergovernmental Panel on Climate Change (IPCC), human activities have affected the climate to various degrees in different ways. Compared to pre-industrialization levels (1850–1900), the increase in global temperature from 2010 to 2019 was about 0.8–1.3 °C, which has had a profound impact on social development [5].

The Qinling Mountains (QMs), located predominantly in the south of Shanxi province in central China, are considered to be a division in geology, geochemistry, and physical geography between northern China and southern China [6]. Furthermore, as an important geographical boundary between central and eastern China, the QMs are situated at the edge of the Asian monsoon region and are sensitive to climate change [7,8]. Thus, they represent a climate transition belt where the typical subtropical zone gradually shifts into a warm temperate zone from south to north and the humidity shifts towards a semi-humid zone from east to west [9].

The effects of the QMs on regional climate, especially rainfall and temperature, have been shown to have great scientific relevance for climate change research in China [10–12]. As a key region in the study of regional climate change in China, the changes experienced in the climate elements in the QMs in the past decades have been the research focus of many scholars. In previous studies, both increasing and decreasing trends in annual rainfall have been reported in northwest China [13–15]. Meng et al. [16] indicated a declining trend in annual rainfall in the QMs. Seasonally, a decreasing trend was also observed in spring and autumn, while increasing trends were observed in summer and winter. Spring and autumn rainfall significantly contributed to this observed decline in annual rainfall. Li et al. [17] concluded that the intensity of extreme rainfall increased in the Qinling–Daba Mountains. Shao et al. [18] pointed out that most extreme rainfall indices decreased in spring, autumn, and winter and increased in summer in the Qinling–Daba Mountains. Li et al. [6] revealed that the Qinling–Daba Mountains have an obvious effect on both the spatial–temporal distribution and diurnal cycle of regional rainfall. Zhang et al. [4] used CMIP 6 data to estimate future rainfall changes in the QMs and revealed the basic characteristics of the atmospheric water cycle in mountainous areas under the action of monsoons as well as the temporal and spatial variation mechanisms of water resources in the "central water tower".

Mo et al. [19] simulated the temperature field in the QMs by constructing a digital elevation model (DEM) map. Liu et al. [20] analyzed and compared the temperature of the QMs over the past 200 years using the tree ring statistical method. Bai et al. [21] concluded that the isotherm found in January in the QMs has gradually moved northward in the past 50 years. Bai et al. [22] found that the trend of climate change and the time points of abrupt climate change were consistent over the northern and southern slopes in the QMs. Li et al. [23] indicated that the total rainfall amount has decreased, whereas the amount of extreme rainfall has increased, based on eight extreme rainfall indexes in the northern and southern QMs. According to the study of Zhang et al. [24], the rainfall in the QMs has shown a downward trend in the last 50 years, and the 800 mm rainfall contour line has clearly moved. Zhang et al. [25] found that the rainfall belt in the QMs has moved over the last 40 years compared with the standard period. The study of Gao et al. [26] showed that the climate in the QMs has undergone a warming and humidifying trend.

In addition, these studies on climate change in the QMs are mainly based on the data obtained from more than 30 meteorological stations in recent years, and different results show that the temperature has undergone an upward shift [25,27,28]. Furthermore, there is a huge elevation difference of more than 3000 m in the QMs, and the meteorological data for the high-elevation regions are based on the conventional vertical lapse rate of temperature and the data derived from low-altitude stations. However, these extrapolation methods cannot fully reflect the complex variability in temperature and rainfall in the QMs, and it is necessary to obtain data from higher-elevation stations for supplementary correction [29].

Therefore, studying the rules of trends, as well as their attributions at different altitudes and different time scales in the QMs, is essential to exploring climate change in China. In this study, climate trend analysis, mutation tests, spatial interpolation, etc., were applied to determine the rainfall and temperature trends as well as their hidden values and to analyze the correlations with geographic factors, such as altitude, longitude, and latitude in the QMs so as to determine the influence of geographical factors on mountain climate. The aim of the work is to understand the response of regional climate change to global warming; the results of this study will enhance the scientific basis of guidelines regarding

how to deal with future climate change and promoting sustainable development and ecological protection.

This paper is organized as follows: The details of the datasets and methodology are given in the Materials and Methods section. The rainfall and temperature trends on annual and seasonal scales, and analyses of their correlations with geographic factors, are given in the Results section. The Discussion and Conclusions sections are given at the end.

2. Data and Methods

2.1. Data

In this study, the QM region refers to the mountains between the Weihe River and the Hanjiang River in the south of Shaanxi Province, bounded by the Bahe River and the Danjiang River Valley in the east and ending at the Jialing River in the west. The range of the QMs is 32.42° N–35.27° N, 103.8° E–113.07° E. We used the daily and monthly mean temperature and rainfall gauge data from 32 national surface weather stations during the period 1961–2021 and annual mean temperature and rainfall gauge data from 406 regional automated stations during the period 2020–2021. All the data were used to analyze climate change in the QMs and were subjected to quality control (QC). The QC procedures for the current gauge data include the station information check, the missing value and eigenvalue check, the time consistency check, the climate extreme value behavior check, the spatial consistency check, and the interior consistency check. The spatial distribution of meteorological stations and the study area are shown in Figure 1. DEM data at a 30 m resolution were downloaded from the National Science Data Mirroring Website of the Computer Network Information Center, Chinese Academy of Science (http://www.gscloud.cn, accessed on 1 March 2022) [30]. Moreover, the periods of March–May, June–August, September–November, and December–February represent spring, summer, autumn, and winter, respectively.
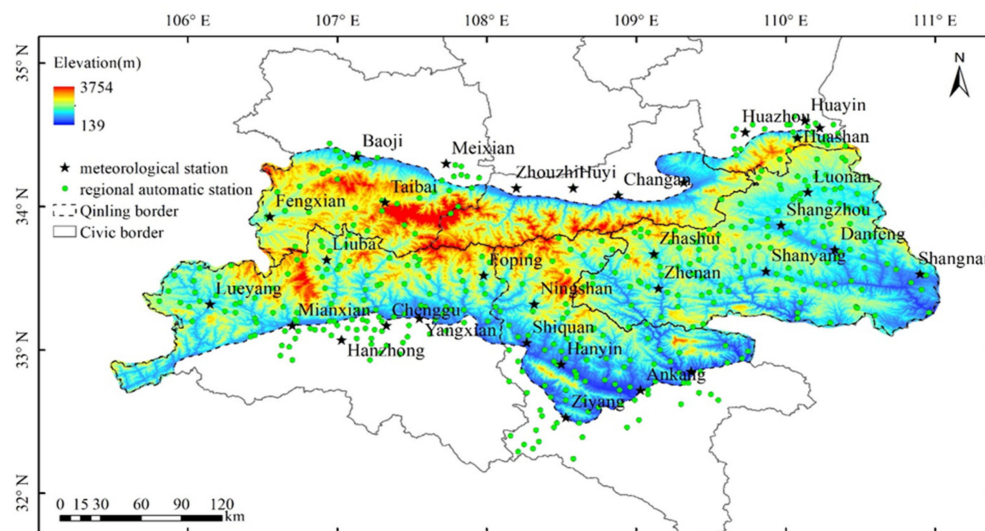

Figure 1. Spatial distribution of meteorological stations in the Qinling Mountains.

2.2. Methods

2.2.1. Climate Trend Analysis

The function of climate trend analysis is primarily to calculate and analyze the tendencies and rates of meteorological elements via the following formula [31]:

$$Y_i = a_0 + a_1 t_1 \tag{1}$$

In this study, Y_i is the value of the meteorological element, t_1 is the time (1961–2021), a_1 is the linear trend (that is, the annual climate tendency rate), and a_0 is the constant term.

2.2.2. Mann–Kendall (M-K) Test

The Mann–Kendall (M-K) method is a detection method on the basis of non-parametric statistics proposed by Mann et al. [32] and Kendall et al. [33]. It can infer overall distribution through the analysis of sample data, introducing the inverse sequence calculation, which can be applied to the detection of the mutation and can reflect the exact location of the mutations [34]. It is widely employed to detect monotonic trends in the time series of hydrometeorological variables, including temperature [35], streamflow [36], and rainfall [37]. This method does not require that the detected data adhere to a specific distribution, and as such, this method requires no assumptions about the data that need to be tested [34].

In this study, the M-K method is used to test the abrupt change in temperature and rainfall series. Its principle is to construct a rank sequence S_k in chronological order for element sequence x:

$$S_k = \sum_{i=1}^{k} r_i, \qquad k = 2, 3, \cdots, n \tag{2}$$

where

$$r_i = \begin{cases} 1, & for\ x_i > x_j, \\ 0, & for\ x_i \leq x_j, \end{cases} \qquad j = 1, 2, \cdots, i.$$

The statistics UF_k are defined under the assumption of random independence of time series:

$$UF_k = \frac{|S_k - E(S_k)|}{\sqrt{var(S_k)}} \tag{3}$$

where $UF_1 = 0$, $E(S_k)$, is the mean of the cumulative S_k; $var(S_k)$ is the variance of the cumulative S_k.

$$\begin{cases} E(S_k) = \dfrac{k(k-1)}{4}, \\ var(S_k) = \dfrac{k(k-1)(2k+5)}{72}. \end{cases} \tag{4}$$

Variable UF_k obeys normal distribution, and different significance levels are set to determine whether the trend of variable UF_k is significant in the confidence interval. The element sequence x is arranged in reverse chronological order, and the above process is repeated with $UB_k = -UF_k (k = n, n-1, \cdots, 1)$, $UB_1 = 0$. By analyzing the trend of UF_k and UB_k, the trend of element sequence x can be obtained and the time of its mutation can be determined. If $UF_k > 0$, it indicates that the sequence tends to rise; otherwise, it declines. If the values of UF_k and UB_k are greater than the critical value of a significance level, the sequence shows a significant trend. If there is an intersection point between UF_k and UB_k, the position of the intersection point is the place at which the mutation occurs [38]. However, this method has some drawbacks. In the case of multiple mutation points or multiple scale mutations in the sequence, this method is not suitable to be applied [34].

2.2.3. Running *t*-Test

Considering some disadvantages of the Mann–Kendall test, we also used the running *t*-test method to test the abrupt change of temperature and rainfall series at the same time. The basic idea of the running *t*-test is based on the significance test; to determine if two samples will occur as mutations, one must analyze whether the difference in the two samples' mean values is obvious or not [34]. If the difference is greater than the given significance level, the two samples exist with obvious qualitative changes.

The principle of this operation is as follows: x is the time series, and n is the number of samples; a certain time point is artificially set as the reference point, and n_1 and n_2 are the numbers of samples before (x_1) and after (x_2) the reference point; t meets the distribution

of $t(n_1 + n_2 - 2)$. $\overline{x_1}$ and $\overline{x_2}$ are the mean values of x_1 and x_2, respectively; S_1^2 and S_2^2 are the variances of x_1 and x_2, respectively. The test statistics (t) are calculated as follows [34,38]:

$$t = \frac{\overline{x_1} - \overline{x_2}}{S\sqrt{\frac{1}{n_1} + \frac{1}{n_2}}} \sim t(n_1 + n_2 - 2) \tag{5}$$

$$S = \sqrt{\frac{(n_1 - 1)S_1^2 + (n_2 - 1)S_2^2}{n_1 + n_2 - 2}} \tag{6}$$

For a significance level of α, we can calculate the test statistic t_α, and if $|t| > t_\alpha$, a mutation exists. However, according to the descriptive analysis of test methods and the previous research experience, the running *t*-test is relatively appropriate for the recognition of mean value type mutations [34,38].

2.2.4. Kriging Interpolation

Kriging interpolation is the method of interpolation deriving from regionalized variable theory, it is a geostatistical interpolation method and an optimal method for estimating regional spatial differences based on the spatial variation of the property in terms of the variogram [39–41]. Kriging interpolation obtains the estimated values of unknown points using known point data by considering the spatial relationship between sample points, using the variogram calculation and structural information. There is no boundary effect in the region and the output surface is smooth. The formula of calculation is as follows [39,41–43]:

$$Z(x_0) = \sum_{i=1}^{k} \lambda_i Z(x_i) \tag{7}$$

where $Z(x_0)$ is the estimated value of the meteorological point; λ_i is the weight coefficient of the measured sample point i; $Z(x_i)$ is the value of the known meteorological station. Kriging interpolation is widely used in the study of variables with spatial correlation [44–46].

In this study, monthly and annual $0.1° \times 0.1°$ grid data are generated using Kriging interpolation, and a correlation analysis between temperature, precipitation data, and the geographical factors is subsequently applied. Statistical significance has been assessed using Student's *t*-test. All the significance values are at the 95% confidence level unless otherwise stated.

3. Results

3.1. Temporal Characteristics of Temperature and Rainfall

3.1.1. Interannual and Interdecadal

The time series of regionally averaged annual mean temperature (AMT) (Figure 2) in the QMs during the period from 1961–2021 shows that the AMT in the QMs has increased significantly over the past 61 years, and the temperature tendency rate (TTR) is 0.22 °C/10a ($p = 0.05$). The maximum annual temperature was 14.4 °C, which occurred in 2013. In that year, an anomalous long-term high temperature occurred in the QMs, the subtropical high was stronger to the north (Figures not shown), and the atmospheric circulation anomaly may be the reason for the temperature increase in the QMs [47]. On the other hand, the minimum value was 12.2 °C, which occurred in 1984. In that year, the La Niña event triggered a strong East Asian winter monsoon, the Siberian high pressure was strengthened, and the cold air was active in East Asia (Figures not shown), so the minimum temperature occurred in the QMs [48,49]. According to the five-year moving mean temperature, the upward trend of temperature was relatively slow before the 1980s, and the TTR value was 0.09 °C/10a. Then, the AMT gradually increased from the 1980s, and the TTR was 0.54 °C/10a during the period 1981–1998. After that, the increasing trend slowed down, and the TTR was 0.13 °C/10a during the period 1999–2021.
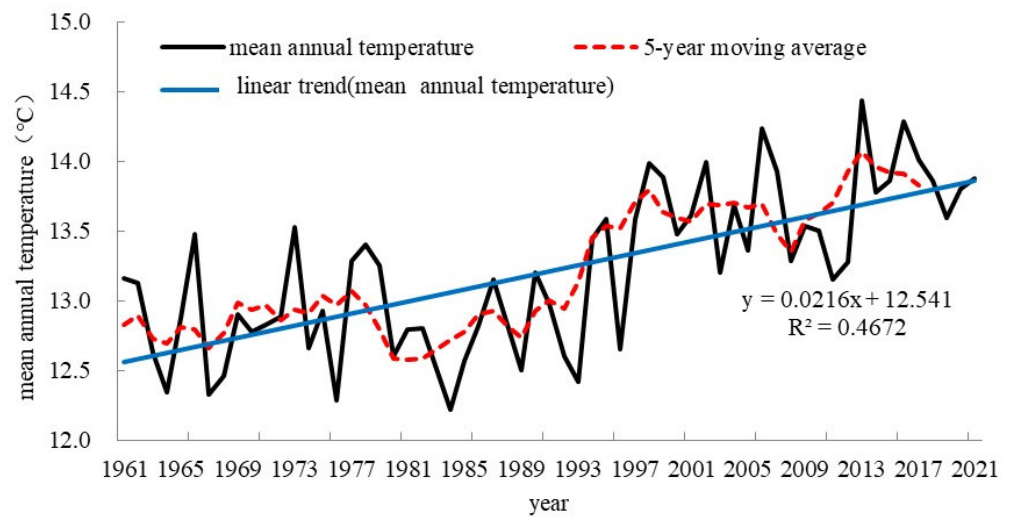
Figure 2. Time series of regionally averaged annual mean temperature (AMT) (unit: °C) from 32 stations in the QMs during the period 1961–2021. The black line denotes the temperature curve, the red dashed line denotes the 5-year moving average curve, and the blue line denotes the linear trend curve.

Figure 3 shows the time series of regionally averaged annual mean rainfall amount (AMRA) in the QMs during the period 1961–2021; it is noted that the trend of AMRA in the QMs over the last 61 years was not significant. The maximum AMRA was 1184.2 mm, which occurred in 2021. In that year, the anomalous plateau upper trough and the anomalous subtropical high affected the rainfall in the QMs [50]. On the other hand, the minimum value was 492.1 mm, which occurred in 1997. In that year, the occurrence of El Niño phenomenon caused the Western Pacific subtropical high to move northward and retreat southward rapidly, which was the reason for the negative rainfall anomaly in the QMs [51]. The variability in types of rainfall is consistent with the variability in AMRA, with large interannual fluctuation, but this trend is not significant (Figures not shown).
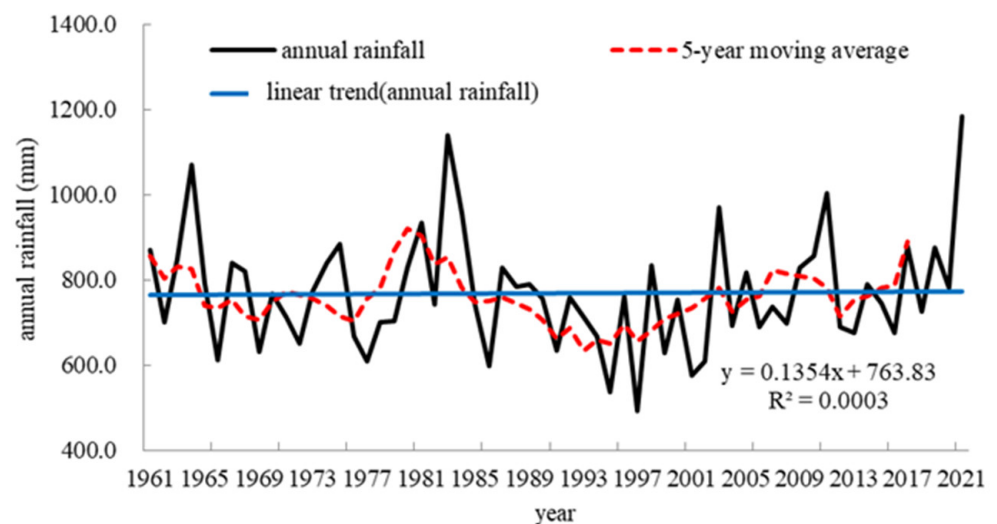

Figure 3. Time series of regionally averaged annual mean rainfall amount (AMRA) (unit: mm) from 32 stations in the QMs during the period 1961–2021. The black line denotes the rainfall curve, the red dashed line denotes the 5-year moving average curve, and the blue line denotes the linear trend curve.

Table 1 shows the interdecadal statistics of regionally averaged AMT in the QMs, indicating that negative temperature anomalies occurred in the 1960s, 1970s, and 1980s. However, a positive temperature anomaly occurred after the 1990s. The differences seen in the temperature anomalies in the 1960s, 1970s, 1980s, and 2010s were 1.0 °C ($p = 0.05$), 0.9 °C ($p = 0.05$), and 1.1 °C ($p = 0.05$), respectively. This indicates that the temperature has increased significantly across the QMs in the past 51 years.

Table 1. The regionally averaged AMT in QMs for different periods.

Variable	1960s	1970s	1980s	1990s	2000s	2010s
AMT (°C)	12.8	13.0	12.7	13.3	13.6	13.8
AMT anomaly (°C)	−0.4	−0.2	−0.5	0.1	0.4	0.6

To further understand the features of rainfall, we have examined the different classifications of rainfall in the QM region. Here, we have divided the daily rainfall into five types: light rainfall (LR; 0.1–9.9 mm), moderate rainfall (MR; 10.0–24.9 mm), heavy rainfall (HR; 25.0–49.9 mm), torrential rainfall (TR; 50.0–99.9 mm), and downpour rainfall (DR; ≥100.0 mm); after this, we calculated the monthly mean values of LR, MR, HR, TR, and DR during the period from 1961–2021.

As shown in Table 2, regarding the regionally averaged differences in types of rainfall in the QMs during the period from 1961–2021, the MR type represents the maximum proportion, accounting for 27.9% of the AMRA, while the TR type represents the minimum proportion, accounting for 12.8% of the AMRA. Moreover, LR, HR, and DR accounted for 24.0%, 21.5%, and 13.8%, respectively.

Table 2. The regionally averaged light rainfall (LR), moderate rainfall (MR), heavy rainfall (HR), torrential rainfall (TR), and downpour rainfall (DR) in the QMs during the period 1961–2021.

Period (Years)	LR (mm)	MR (mm)	HR (mm)	TR (mm)	DR (mm)
1961–2021	218.9	254.3	196.2	116.9	125.4

As shown in Table 3, positive AMRA anomalies occurred in the 1960s, 1980s, and 2010s, and the value of the difference exceeded 50 mm in the 1980s. Negative AMRA anomalies occurred in the 1970s, 1990s, and 2000s, and the value of the difference was −76.4 mm in the 1990s. The AMRA significantly decreased by 130.1 mm from the 1980s to 1990s, accounting for 13.5% in the 1980s; this indicates a declining trend in the AMRA in the QMs from the 1980s to the 1990s, which is also supported by previous studies, which reported an obvious change in the QMs after the 1980s, with a declining rainfall trend over the QMs [16]. In addition, a trend of increase in the AMRA was seen from the 1990s to 2010s, and it accounted for 13.0% in the 1990s. Furthermore, a positive LR anomaly occurred during the period 1960–1980, after which a negative LR anomaly occurred. Negative MR and TR anomalies occurred in the 1990s and 2000s, and positive anomalies occurred in the 2010s. Negative HR and TR anomalies occurred in the 1990s, and positive anomalies occurred after the 2000s. The above analysis shows that the increase in the AMRA across the QMs in the 2010s was mainly caused by increases in MR, HR, TR, and DR; in addition, the LR had been lower than the mean rainfall since the 1990s.

According to the above analysis, the results suggest that the annual rainfall trend was declining in the QMs before the 2000s; this result is consistent with those of Meng et al. [52] and Wang et al. [14]. In addition, we found an increasing trend in the AMRA in the QMs from the 1990s to the 2010s and a declining trend from the 1980s to the 1990s. Global warming [53], Pacific decadal oscillation (PDO) [53], Atlantic multidecadal oscillation (AMO) [53], and Asian–Pacific oscillation (APO) [54] might be the reason for AMRA change in the QMs.

Table 3. The regionally averaged annual mean rainfall amount (AMRA), light rainfall (LR), moderate rainfall (MR), heavy rainfall (HR), torrential rainfall (TR), and downpour rainfall (DR) in the QMs in different periods.

Variable	1960s	1970s	1980s	1990s	2000s	2010s
AMRA (mm)	941.9	885.8	965.5	835.4	898.4	943.9
AMRA anomaly (mm)	30.1	−26.0	53.7	−76.4	−13.5	32.1
LR (mm)	236.0	219.3	227.7	203.2	214.6	212.8
LR anomaly (mm)	17.1	0.4	8.8	−15.7	−4.4	−6.2
MR (mm)	279.7	246.4	266.3	233.4	240.7	259.5
MR anomaly (mm)	25.5	−7.9	12.1	−20.8	−14.2	5.3
HR (mm)	195.3	180.1	219.8	167.5	199.1	215.5
HR anomaly (mm)	−0.9	−16.1	23.6	−28.7	2.9	19.2
TR (mm)	111.6	112.4	131.1	109.3	112.2	125.0
TR anomaly (mm)	−5.3	−4.5	14.1	−7.7	−4.7	8.1
DR (mm)	119.3	127.6	120.6	122.0	131.8	131.1
DR anomaly (mm)	−6.1	2.2	−4.8	−3.4	6.4	5.7

3.1.2. Seasonal

To further determine the seasonal features of temperature and rainfall, we have examined the different seasonal features of AMT and AMRA in the QMs (Table 4). The results show that the AMT increased from spring to winter, and the tendency rates were 0.33 °C/10a ($p = 0.01$), 0.07 °C/10a, 0.20 °C/10a ($p = 0.05$) and 0.28 °C/10a ($p = 0.05$), respectively. The maximum increase in AMT occurred in spring, and the minimum occurred in summer. In addition, the polar vorticity index and Atlantic SST index were the most relevant circulation index and climate index, respectively, to seasonal AMT. These two indices revealed the trend of climate warming in the past 50 years and might be related to the significant warming in the QMs [55]. Furthermore, the significant warming might also be associated with the warm phase of Atlantic multidecadal oscillation (AMO) [56].

Table 4. The regionally averaged AMT and AMRA in the QMs during different seasons in the period 1961–2021.

Variable	Spring	Summer	Autumn	Winter
AMT (°C)	13.8	23.9	13.2	2.0
Tendency rate (°C/10a)	0.33 ***	0.07	0.20 **	0.28 **
AMRA (mm)	240.0	512.9	401.0	34.8
Tendency rate (mm/10a)	−6.35	8.14	−1.10	0.66
LR (mm)	61.2	68.9	69.0	20.3
LR tendency rate (mm/10a)	−1.77	−1.53	−1.46	0.06
MR (mm)	66.1	107.0	80.3	14.5
MR tendency rate (mm/10a)	−3.36	2.06	−2.78	0.10
HR (mm)	48.6	113.5	70.6	–
HR tendency rate (mm/10a)	−0.83	3.03	0.33	–
TR (mm)	64.1	98.8	72.9	–
TR tendency rate (mm/10a)	−0.36	2.06	0.41	–
DR (mm)	–	124.7	108.1	–
DR tendency rate (mm/10a)	–	1.16	–	–

(Note: the superscript "*" indicates the following—*** $p = 0.01$, ** $p = 0.05$; the 10a stands for 10 years).

Furthermore, the trend of increase in the AMRA manifested in winter and summer in the QMs, with the maximum increase in summer and the minimum increase in winter. In spring and autumn, decreases in AMRA occurred, with the maximum decreasing trend seen in spring and the minimum decreasing trend seen in autumn. Zuo et al. [57] and Zhao et al. [58] noted that the spring AMRA decreased in the QMs might be caused by a

significant decrease in snow cover in Eurasia and a strengthening northerly wind from East Asia in spring. Gu et al. [59] indicated that the decrease in AMRA in autumn in the QMs might be closely related to SST anomalies in the tropical Pacific. In addition, the increased AMRA in winter and summer were related to global warming, Pacific decadal oscillation (PDO), and Atlantic multidecadal oscillation (AMO) [53]. Regarding the seasonal distributions of the different types of rainfall, MR, HR, TR, and DR showed increasing trends in summer, but LR did not, so we can infer that the increase in AMRA in summer was mainly caused by the increases in MR, HR, TR, and DR. In winter, LR and MR showed increasing trends. In spring, MR, HR, TR, and DR showed decreasing trends, which is consistent with the decreasing trend of AMRA. In autumn, LR and MR showed decreasing trends, while HR and TR showed increasing trends; as such, we can infer that the decrease in AMRA in autumn was mainly caused by the decreases in LR and MR. Moreover, the change in temperature and specific humidity in the lower atmosphere were strongly associated with the decrease in the frequency of LR occurred in summer. The increasing temperature was considered to reduce the frequency of LR occurred [60].

In addition, previous studies suggested that the annual and seasonal rainfall in the QMs was influenced by climate anomalies and geographical factors [61], which could be due to atmospheric circulation anomalies, the Asian monsoon anomaly, or a combination of factors (i.e., vegetation cover percentage, direction of slope, degree of slope, and so on) [62,63].

3.2. Spatial Characteristics of Temperature and Rainfall

3.2.1. Spatial Distribution of Temperature

Figure 4A shows a "dipole-type" spatial pattern in the AMT, which was distributed from southeast to northwest in the QMs. The highest AMT was measured in Ankang and its neighboring regions, with maximum values of above 15 °C. Mean temperatures of 14.0–15.0 °C were measured in Mianxian, Yangxian, Hanzhong, Shangnan, Shangluo, and Danfeng. Taibai in the northwestern region of the QMs and Luonan in the northeast yielded the minimum AMT, with values of about 8.0 °C; the difference between the maximum and minimum AMT was about 7.0 °C. In the QM region, the AMT showed an increasing trend (Figure 4B). The greatest increases in AMT occurred in Zhen'an, Zhashui, Fuping, and Baoji, with a rate of over 0.3 °C/10a, and the smallest increases were measured in Shiquan, Ankang, Hanyin, and Ziyang, primarily distributed in the southern region of the QMs, with increase rates below 0.1 °C/10a. The above results show obvious regional differences in the increases in AMT; the increase rate was higher in the northwestern and central regions of the QMs and could be associated with Figure 1 for elevation. That is, the AMT increase rate appeared to be greater at higher elevations, which was basically consistent with the analysis results of Dong et al. [64].

Over the past 50 years, the changing temperature trends over the northern and southern regions of the QMs have been obvious and synchronous, with the warming process manifesting a "non-smooth, nonlinear, and ladder-shaped" pattern. The spatial variation in temperature is characterized by "synchronous warming and differential north–south change" [63]. The QM region displays differences in temperature in response to global warming over the north and south. The northern boundary of the north subtropical zone extends upwards along the southern QMs, whereas the warming zone extends in the form of an enclave into the northern QMs due to rapid urbanization and mountain blocking [63,65].

3.2.2. Spatial Distribution of Rainfall

As can be seen in Figure 5A, the greatest AMRA was measured in the southwest, while lower levels occurred in the northeast of the QMs. The maximum AMRA values were measured in Foping, Ningshan, Shiquan, Hanyin, and Ziyang, which were above 1000 mm. On the contrary, the minimum AMRA values were measured in Baoji, Xi'an, and Weinan, located in the north of the QMs, and were below 600 mm. The difference between the maximum and minimum AMRA was over 400 mm. The maximum trends of increase

in AMRA were measured in Shangnan and Danfeng, with rates of 10.1–18.8 mm/10a (Figure 5B).
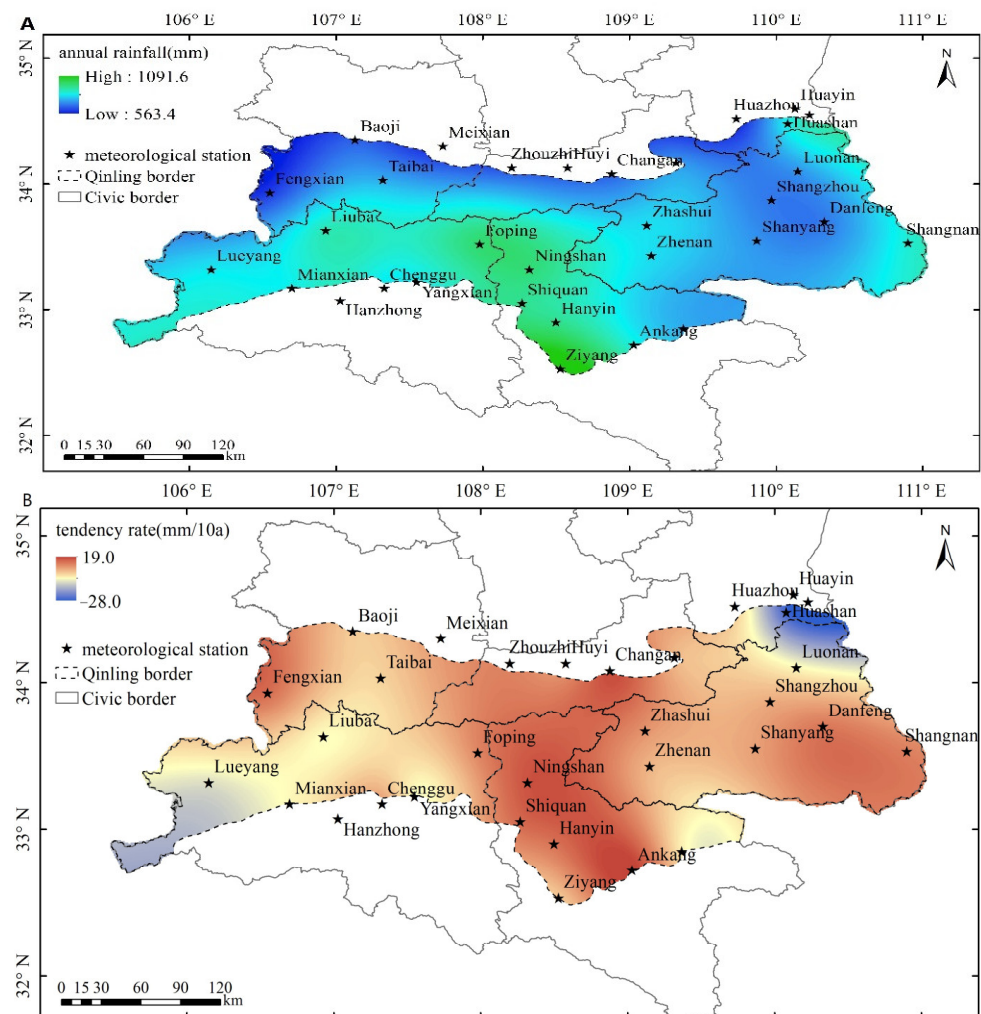

Figure 4. (**A**) The spatial distribution of AMT (unit: °C) in the QMs averaged from 1961 to 2021. (**B**) The spatial distribution of linear variation in AMT trends (unit: °C/10a) in the QMs.

As shown in Figure 6, the greatest distribution of LR occurred in the southwest of the QMs, and the least occurred in the northeast. The total amount of LR type in the QM region was above 170.8 mm, with the highest measurements in Liuba, Ziyang, Foping, and Ningshan and the smallest in Huayin, Huazhou, and Tongguan. More MR type was measured in the central QM region, and less occurred in the eastern and western regions; its total value was above 195.6 mm, with the highest values measured in Ankang and Foping in the east of Hanzhong and Zhashui and Zhen'an in the west of Shangluo. The smallest values measured were in the west of Baoji and the east of Shangluo. More HR and TR were measured in the south of the QMs, and less were measured in the remaining regions; the highest values occurred in Ziyang, Foping, Ningshan, and Hanyin, and the smallest values occurred in the north and east of the QMs. In addition, a decreasing LR trend was seen across most of the QM region, while increasing trends were seen in Zhashui and Chenggu. The increases in MR, HR, and TR occurred in the central QM region, with decreases in the remaining regions.
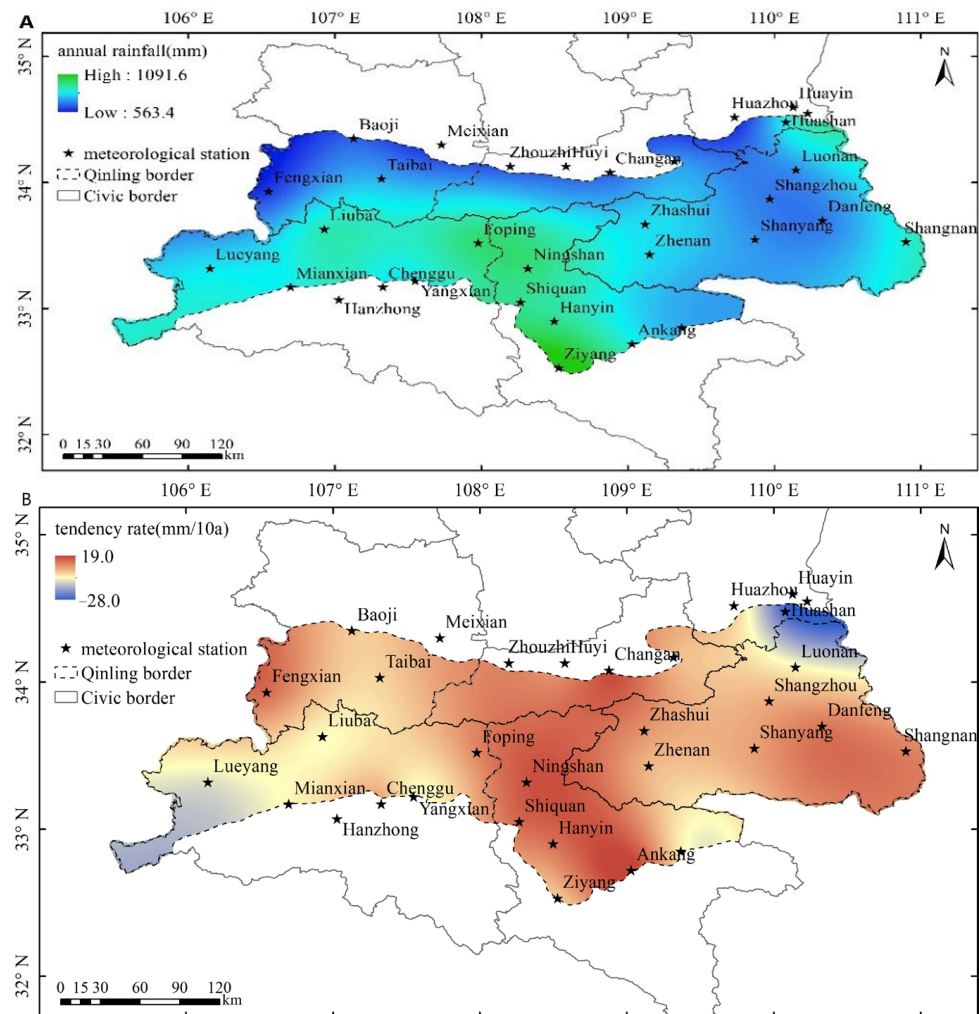
Figure 5. As in Figure 4, but for AMRA (**A**) (unit: mm) and AMRA trends (**B**) (unit: mm/10a).

3.3. The Abrupt Changes in Temperature and Rainfall

In this study, we used the M-K test and running *t*-test to examine dramatic changes in the spatiotemporal characteristics of temperature. As can be seen from the results of the M-K test (Figure 7A) and running *t*-test (Figure 7B) applied to the AMT time series across the QMs, the most abrupt change occurred in 1997—that is, a significant shift in the AMT occurred in 1997. The AMT showed an increasing trend after 1997. In fact, the most significant increase trend was seen after 2002 ($p = 0.05$), signifying that the AMT in the QMs has increased significantly since this time. In 1997, the occurrence of El Niño phenomenon led to a global atmospheric circulation anomaly, subtropical high anomaly, and hot and dry weather [51]. After that, solar activity, volcanic activity, human factors, greenhouse gas emissions, and land use changes played a major role in climate warming, and the increase in AMT in the QMs continued [66]. It can be seen from Figure 8, regarding the M-K test (Figure 8A) and running *t*-test (Figure 8B) applied to the annual DR time series across the QMs, that the year of most abrupt change was 1984; that is, a significant shift in the annual DR occurred in 1984. The rainfall anomaly in the QMs might be associated with sea surface temperature (SST) anomaly over the central-eastern equatorial Pacific and the North Atlantic [67]. In 1984, an SST anomaly occurred in the east-central equatorial Pacific, accompanied by the Walker circulation and meridional circulation anomalies. Additionally, the DR increased in the QMs [67]. In addition, the time series of AMRA, LR, MR, and HR showed no obvious year of abrupt change (Figures not shown), and they generally remained stable. Other previous studies have indicated that various external forcing factors,

such as solar radiation, greenhouse gases, and land use, could cause the abrupt changes in the QMs during the period from 1961−2021 [68].
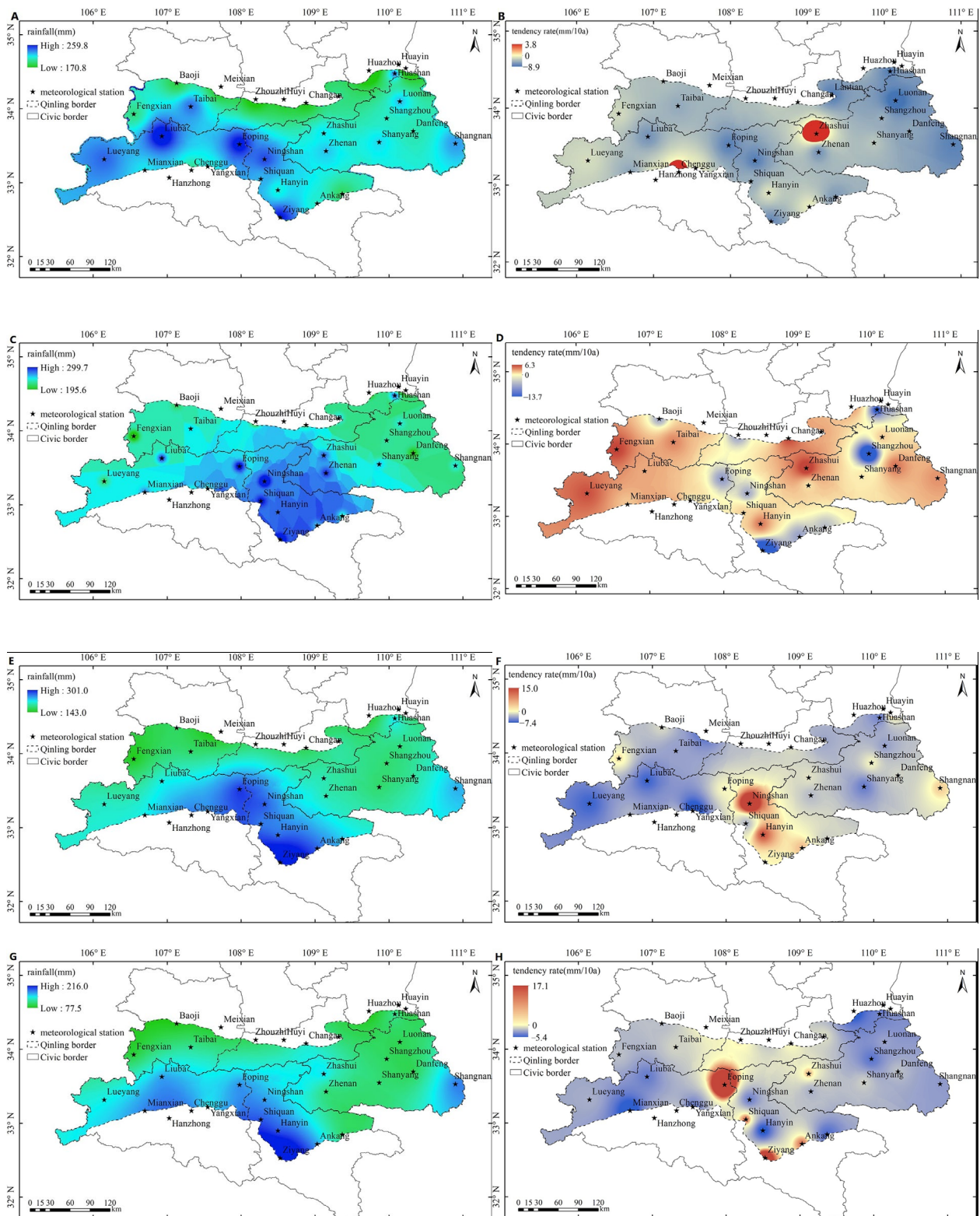

Figure 6. As in Figure 5A, but for LR (**A**), MR (**C**), HR (**E**), and TR (**G**) (unit: mm). As in Figure 5B, but for LR (**B**), MR (**D**), HR (**F**), and TR (**H**) trends (unit: mm/10a).

A

Mann-Kendal test

B
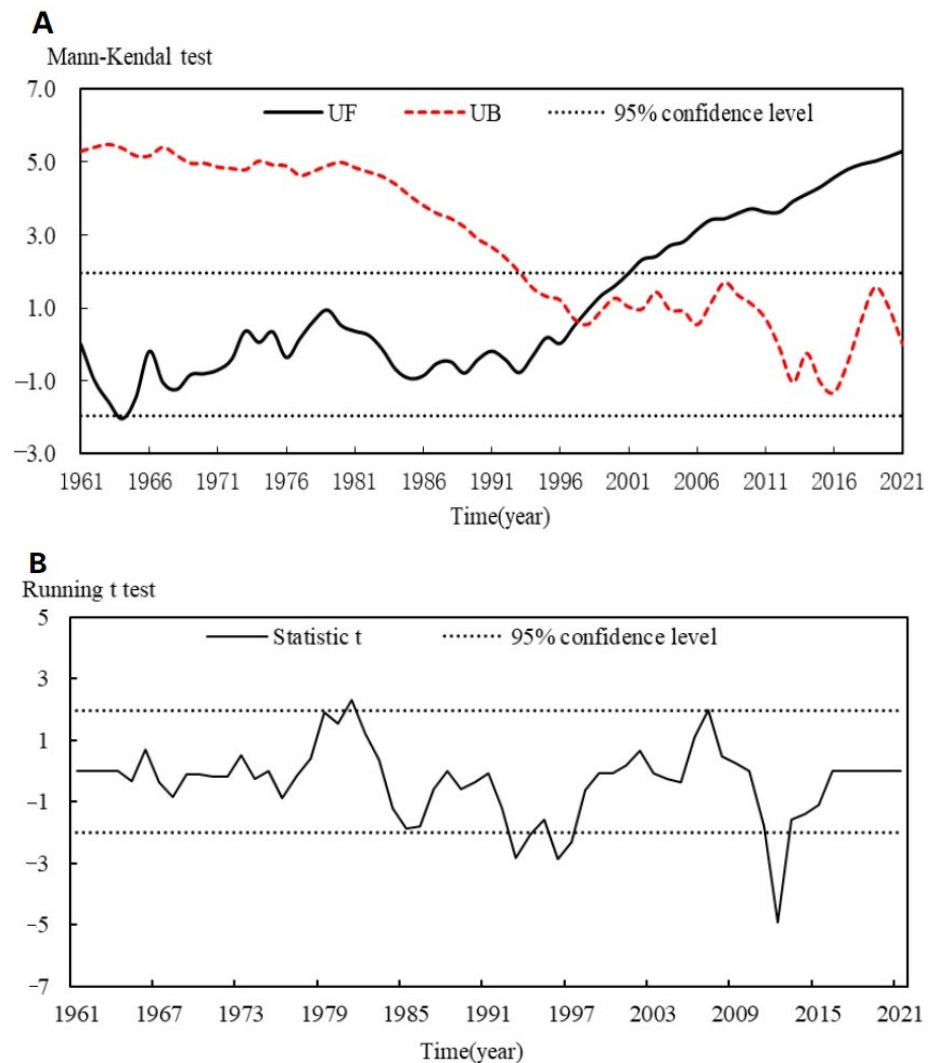
Running t test

Figure 7. Mann–Kendall (**A**) and running *t*-tests (**B**) for the time series of the AMT over the QMs during the period from 1961−2021. The two black dashed lines indicate the 95% confidence level of the two tests. In (**A**), the black line denotes the sequential statistical curve, UF, and the red dashed line denotes the reverse statistical curve, UB. The black lines in (**B**) denote the sequential statistical curve t.

3.4. Correlation Analysis between Temperature, Rainfall, and Geographical Factors

3.4.1. Correlation Analysis of Temperature, Rainfall, and Elevation

In order to better understand the distribution and variation of temperature and rainfall in the QMs, we used the research methods of Huang et al. [69] and Bi [70] to analyze the correlation between AMT and AMRA with geographic factors in this paper. The correlation coefficients of AMT and AMRA with altitude, longitude, and latitude and the variation characteristics of AMT and AMRA with geographical factors were studied. Since the highest elevation of the QMs is over 3700 m and the highest national meteorological station is 2064.9 m, we combined the data from regional automatic stations with data from the national station to complete the spatial interpolation analysis. This better reflects the actual distribution of meteorological elements in the high-elevation region, helping us to understand the relationship between temperature, rainfall, and geographical elements.
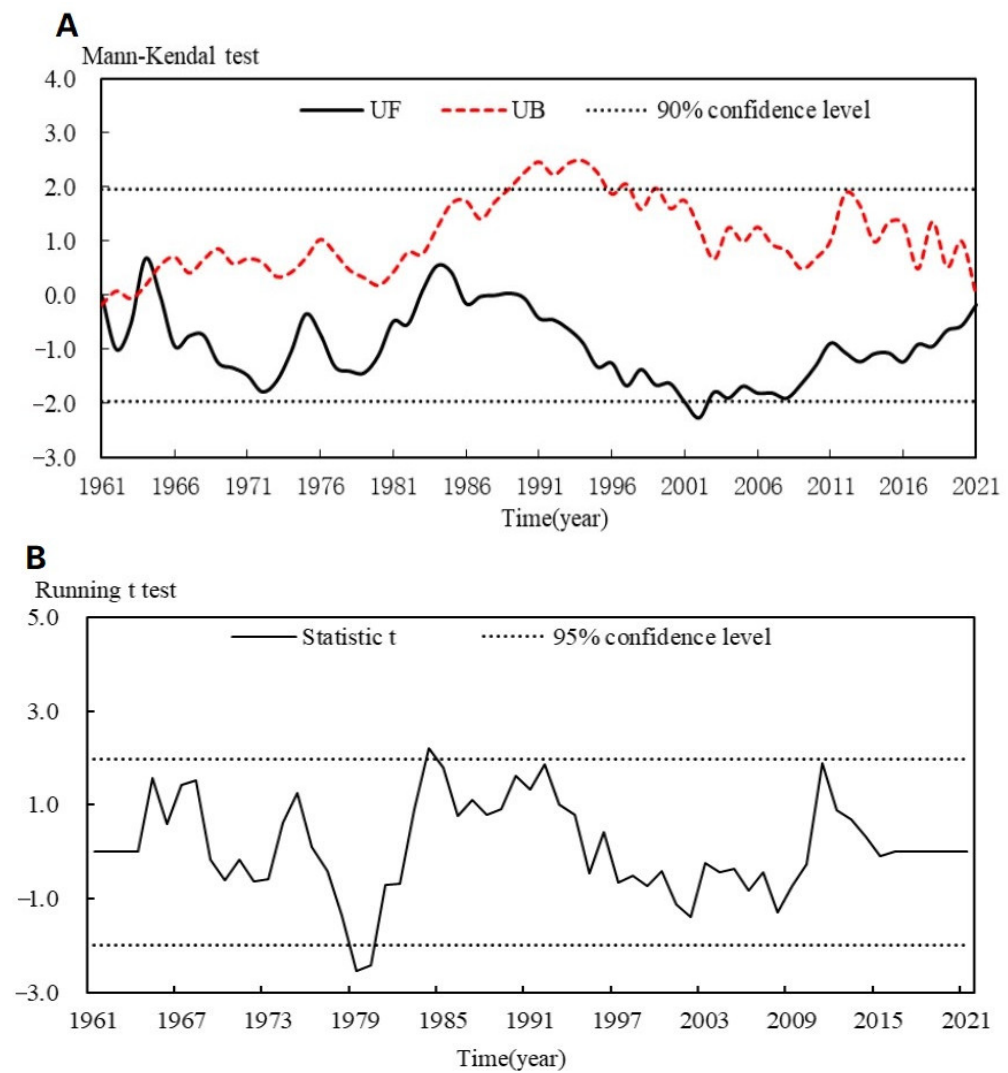
A

B

Figure 8. As in Figure 7, but for DR.

As can be seen from Table 5, there was a significant negative correlation between AMT and elevation, with a correlation coefficient of −0.700 ($p = 0.01$). On the other hand, the correlation coefficient between AMRA and elevation was significantly positive, with a value of 0.142 ($p = 0.01$). Furthermore, there was a significant positive correlation between AMT and longitude, with a correlation coefficient of 0.147 ($p = 0.01$). The correlation coefficient between AMRA and longitude was significantly negative, with a value of −0.233 ($p = 0.01$). In addition, there was a significant negative correlation of AMT and AMRA with latitude, with correlation coefficients of −0.617 ($p = 0.01$) and −0.868 ($p = 0.01$).

Table 5. Correlation coefficient between the AMT and AMRA and various geographical factors in the QMs during the period from 1961–2021.

	Elevation (m)	Longitude (°E)	Latitude (°N)
AMT (°C)	−0.700 ***	0.147 ***	−0.617 ***
AMRA (mm)	0.142 ***	−0.233 ***	−0.868 ***

(Note: the superscript "*" indicates the following—*** $p = 0.01$).

In order to explore the changes in air temperature and rainfall with elevation in greater detail, the mean temperature and rainfall within the corresponding elevation ranges were calculated at intervals of 100 m [69,70]. As Figure 9 shows, the AMT exhibited a decreasing

trend with elevation increase, at a rate of 0.45 °C/100 m (*p* = 0.01). In the elevation range of 0 m (16.4 °C) to 3730 m (−1.6 °C), the mean temperature decreased by 18 °C. In the elevation range of 0 to 2400 m, the temperature decreased slowly as the elevation increased, but above 2400 m, the temperature decreased rapidly. In particular, the maximum temperature decreased as the elevation increased from 3300 to 3700 m.
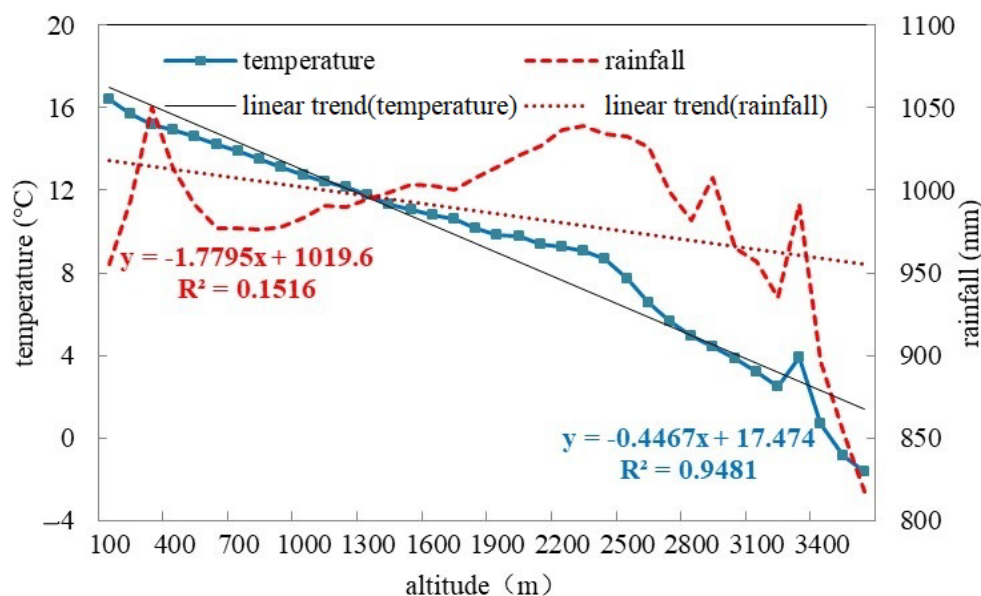

Figure 9. The AMT (unit: °C) and AMRA (unit: mm) change with elevation in the QMs. The brown dashed line denotes the AMRA curve, and the blue dashed line denotes the AMT curve. The black line denotes the linear trend of the temperature curve, and the black dashed line denotes the linear trend of the rainfall curve.

The AMRA showed an increasing trend as the elevation increased. In the elevation range of 0 to 3730 m, the changes in AMRA with increased elevation were more complicated, with an alternating trend of "increase–decrease–increase–decrease". In the elevation range of 200 to 300 m, the maximum AMRA reached was 1050.0 mm. Above 900 m, the AMRA began to increase gradually, and another maximum value was measured at the elevation of 2200 m to 2300 m—1038.8 mm. Then, above 2400 m, as the elevation increased, the AMRA decreased in a fluctuating pattern; in the elevation range of 3600 to 3730 m, the minimum AMRA was 817.6 mm. In addition, the AMRA rapidly dropped above 3400 m. These results signify consistent change trends in the AMT and AMRA with elevation increases, while the AMT and AMRA decreased from low to high elevation in the QM region.

3.4.2. Correlation Analysis of Temperature, Rainfall, and Longitude

In order to explore the changes in air temperature and rainfall at different longitudes in more detail, the mean temperature and rainfall values within corresponding longitudinal ranges were calculated at intervals of 0.2° [69,70]. As can be seen from Figure 10, with changes in longitude, the AMT showed an increasing trend at a rate of 0.04 °C/0.2° (no significant). The minimum temperature was 9.8 °C, which was measured in the longitude range of 107.4°–107.6° E, and the maximum value was 14.4 °C in the longitude range of 110.6°–110.8° E. Furthermore, the AMRA increased in the western QM region and decreased in the east with longitudinal increase. In the longitude range of 107.6°–107.8° E, the maximum AMRA was measured with a value of 1109.2 mm. To the east of 107.8° E, the AMRA showed a decreasing trend, and the minimum value of 875.8 mm appeared in the longitude range of 110.6°–110.8° E. These results further prove that the AMT and AMRA showed different change trends with longitudinal increase; the AMT increased and the AMRA decreased from the west to the east in the QM region.
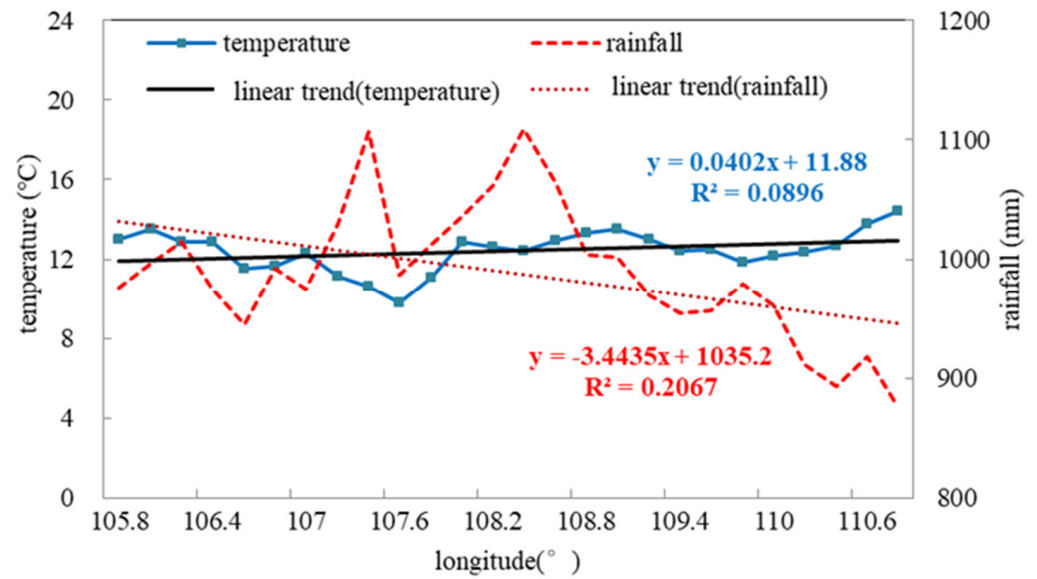
Figure 10. As in Figure 9, but for longitude in the QMs.

3.4.3. Correlation Analysis of Temperature, Rainfall, and Latitude

In order to explore the changes in air temperature and rainfall that occurred with latitude in more detail, the mean values of temperature and rainfall within the corresponding latitude range were calculated at intervals of 0.1° [69,70]. Figure 11 shows that with increases in latitude, the AMT decreased with a linear trend of 0.23 °C/0.1° ($p = 0.01$). The minimum AMT was 10.0 °C, measured at 34° N, and the maximum AMT was 15.9 °C at 32.8° N. Furthermore, with increases in latitude, the AMRA showed a decreasing trend of up to −12.6 mm/0.1° ($p = 0.01$). The minimum AMRA was 842.4 mm, measured at 34.5° N, and the maximum AMRA was 1165.0 mm at 32.5° N. This indicates significant differences in AMRA between the north and south of the QM region. The AMT and AMRA showed consistent change trends with increases in latitude, with both decreasing gradually from the south to the north of the QM region.
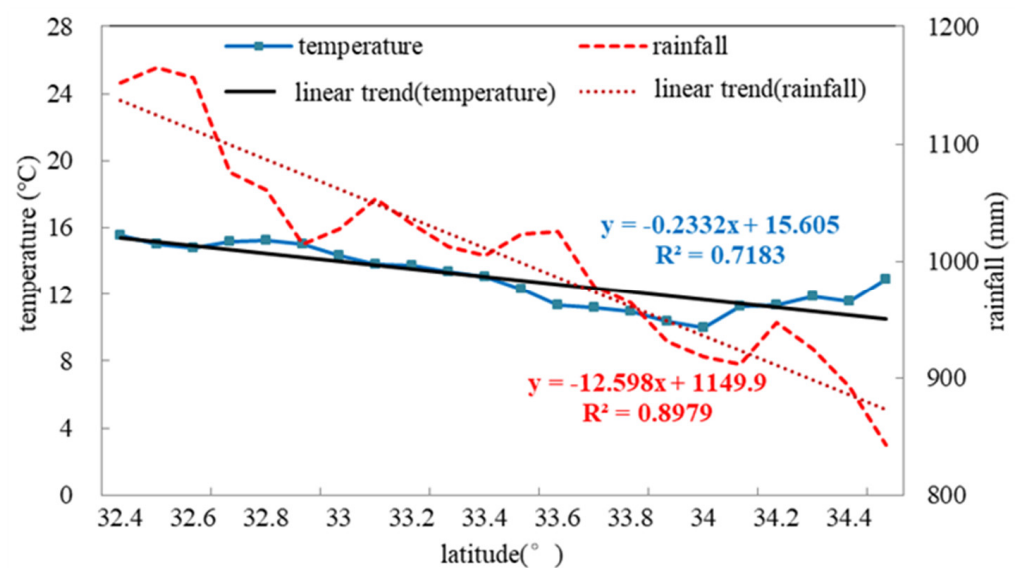

Figure 11. As in Figure 9, but for latitude in the QMs.

4. Discussion and Conclusions

In this study, we investigated the spatiotemporal characteristics of temperature and rainfall in the QMs during the period 1961–2021, and the correlations between temperature and rainfall and geographical factors were studied in detail. The results show that the AMT has significantly increased in the QMs. This increase has been significant in all seasons, with the maximum increasing tendency in spring and the minimum increasing tendency in summer. Positive AMRA anomalies occurred in the 1960s, 1980s, and 2010s, and negative anomalies occurred in the 1970s, 1990s, and 2000s. In the last ten years, MR, HR, TR, and DR showed increasing trends, but LR did not. The AMT increase rate was greater in the northwest and central regions of the QMs, whereas this rate was smaller in the southwestern and eastern regions of the QMs. Considering the elevation distribution of the QMs, the AMT increase rate appeared to be greater at higher elevations, whereas this rate was lower at lower elevations. This result indicates that higher-elevation regions have a more respond positive to climate change than lower-elevation regions [71]. The AMRA showed a decreasing trend in the southwestern and northeastern regions of the QMs, as there were fewer regions with an increasing AMRA trend compared to those where a decreasing AMRA trend occurred.

In the QMs, MR represented the maximum proportion and accounted for 27.9% of the AMRA, whereas TR represented the minimum proportion and accounted for 12.8%. The AMRA significantly decreased by 130.1 mm from the 1980s to the 1990s and accounted for 13.5% of the total in the 1980s. The increase in AMRA in the QMs in the 2010s was mainly caused by the increases in MR, HR, TR, and DR. The years with the most abrupt changes in AMT and DR were 1997 and 1984, respectively, in the QMs. The AMT and AMRA showed consistent change trends with elevation and latitude increases—the AMT and AMRA decreased from a low elevation to high elevation and from the south to the north of the QM region, respectively. The AMT and AMRA showed different change trends with longitude increases—the AMT increased and the AMRA decreased from the west to the east of the QM region.

In this paper, different types of rainfall have been analyzed. Most of the literature has mainly focused on the TR type, indicating that the change trend of TR over the last 50 years has not been obvious, but we suggest an increasing trend in the TR in this century, which is basically consistent with the research conclusions of Kang [45] and Huang et al. [72].

It should be noted that although this study emphasizes the spatiotemporal characteristics of temperature and rainfall in the QMs, several issues remain unclear. For example, the primary limitations of this study are the limited number of surface weather stations in the QMs, the limited duration of the data collection period and the complex topography of the area, which require further exploration the correlation between meteorological factors and geographical factors in the QMs. Furthermore, it was difficult to analyze all the human and natural factors that could affect rainfall and temperature in this area because of the complex topography [16]. Additionally, solar radiation, aerosol, ENSO, and snow depth may also affect rainfall and temperature in the QMs [73]. In the future, studies should focus on the potential physical mechanisms that influence the spatiotemporal distribution characteristics of temperature and rainfall in order to obtain more accurate trends and perform attribution analyses. With increases in observational data, more in-depth research should be carried out on the spatiotemporal distribution characteristics of temperature and rainfall and their correlations with geographical factors. Our results are expected to enhance the understanding of the meteorological background of the QMs.

Author Contributions: Conceptualization, formal analysis, methodology, writing—original draft, and writing—review and editing, Y.L. and R.L.; project administration, Y.S., X.Z., D.L. and L.Z.; supervision, D.L., R.L. and Y.L. All authors have read and agreed to the published version of the manuscript.

References

1. Nijssen, B.; O'Donnell, G.M.; Hamlet, A.F.; Lettenmaier, D.P. Hydrologic sensitivity of global rivers to climate change. *Clim. Chang.* **2001**, *50*, 143–175. [CrossRef]
2. Trenberth, K.E. Atmospheric moisture residence times and cycling: Implications for precipitation rates and climate change. *Clim. Chang.* **1998**, *39*, 667–694. [CrossRef]
3. Babaousmail, H.; Hou, R.; Ayugi, B.; Sian, K.T.C.L.K.; Ojara, M.; Mumo, R.; Chehbouni, A.; Ongoma, V. Future changes in mean and extreme precipitation over the Mediterranean and Sahararegions using bias-corrected CMIP6 models. *Int. J. Climatol.* **2022**, *42*, 7280–7297. [CrossRef]
4. Zhang, Z.; Duan, K.; Liu, H.; Meng, Y.; Chen, R. Spatio-temporal variation of precipitation in the Qinling mountains from 1970 to 2100 based on CMIP6 data. *Sustainability* **2022**, *14*, 8654. [CrossRef]
5. Fan, X.; Qin, Y.Y.; Gao, X. Interpretation of the main conclusions and suggestions of IPCC AR6 working group I report. *Environ. Prot.* **2021**, *49*, 44–48. (In Chinese) [CrossRef]
6. Li, X.; Wang, N.; Wu, Z. Terrain effects on regional precipitation in a warm season over Qinling-Daba mountains in central China. *Atmosphere* **2021**, *12*, 1685. [CrossRef]
7. Yang, F.M.; Wang, N.; Shi, F.; Ljungqvist, F.C.; Wang, S.; Fan, Z. Multi-proxy temperature reconstruction from the West Qinling Mountains, China, for the past 500 years. *PLoS ONE* **2013**, *8*, e57638. [CrossRef] [PubMed]
8. Yang, F.M.; Wang, N.; Shi, F.; Fredrik, C.L.; Zhao, S.; Liu, T. The spatial distribution of precipitation over the West Qinling region, China, AD 1470–2000. *Palaeogeogr. Palaeoclimatol. Palaeoecol.* **2016**, *443*, 278–285. [CrossRef]
9. Deng, C.H.; Bai, H.Y.; Ma, X.P.; Zhao, T.; Gao, S.; Huang, X.Y. Spatiotemporal differences in the climatic growing season in the Qinling Mountains of China under the influence of global warming from 1964 to 2015. *Theor. Appl. Climatol.* **2019**, *138*, 1899–1911. [CrossRef]
10. Liu, K.; Ma, N.X.; Xu, Y.L.; Sun, G.N. Protection and construction of eco-environment in Qinling Mountainous area. *Chin. J. Eco.* **2004**, *23*, 157–160. [CrossRef]
11. Sun, H.; Bai, H.Y.; Zhang, Q.Y.; Ge, X.P.; Zhang, S.H. Responses of vegetation coverage to regional environmental change in the northern and southern Qinling Mountains. *Acta Sci. Circumstantiae* **2009**, *29*, 2635–2641. [CrossRef]
12. Zhou, Q.; Bian, J.J.; Zheng, J.Y. Variation of air temperature and thermal resources in the northern and southern regions of the Qinling Mountains from 1951 to 2009. *Acta Geogr. Sin.* **2011**, *66*, 1211–1218. [CrossRef]
13. Han, X.; Xue, H.; Zhao, C.; Lu, D. The roles of convective and stratiform precipitation in the observed precipitation trends in Northwest China during 1961–2000. *Atmos Res.* **2016**, *169*, 139–146. [CrossRef]
14. Wang, X.; Wang, B.; Xu, X. Effects of large-scale climate anomalieson trends in seasonal precipitation over the Loess Plateau of China from 1961 to 2016. *Ecol Indic.* **2019**, *107*, 105643. [CrossRef]
15. Li, B.; Chen, Y.; Shi, X.; Chen, Z.; Li, W. Temperature and precipitation changes in different environments in the arid region of northwest China. *Theor. Appl. Climatol.* **2013**, *112*, 589–596. [CrossRef]
16. Meng, Q.; Bai, H.Y.; Sarukkalige, R.J.; Fu, G.B.; Jia, W.H.; Zhang, C.H. Annual and seasonal precipitation trends and their attributions in the Qinling Mountains, a climate transitional zone in China. *Theor. Appl. Climatol.* **2021**, *144*, 401–413. [CrossRef]
17. Li, S.; Yang, S.; Liu, X. Spatiotemporal variability of extreme precipitation in north and south of the Qinling-Huaihe region and influencing factors during 1960–2013. *Prog. Geogr.* **2015**, *3*, 354–363. [CrossRef]
18. Shao, Y.; Mu, X.; He, Y.; Sun, W.; Zhao, G.; Gao, P. Spatiotemporal variations of extreme precipitation events at multi-time scales in the Qinling-Daba mountains region, China. *Quat. Int.* **2019**, *525*, 89–102. [CrossRef]

19. Mo, S.G.; Zhang, B.P. Simulation of temperature fields based on DEM in Qinling Mts. *Mountain Res.* **2007**, *25*, 406–411. [CrossRef]

20. Liu, Y.; Liu, N.; Song, H.M.; Cai, Q.F.; Bao, G.; Wang, W.P. Reconstructed mean air temperature from January to July at the divide sampling site in the mid-Qinling Mountains with tree-ring widths. *Adv. Clim. Chang. Res.* **2009**, *5*, 260–265. [CrossRef]

21. Bai, H.Y.; Ma, X.P.; Gao, X.; Hou, Q.L. Variations in January temperature and 0 °C isothermal curve in Qinling Mountains based on DEM. *Acta Geogr. Sin.* **2012**, *11*, 1443–1450. [CrossRef]

22. Bai, J.; Yan, J.P.; Su, K.H. Differential analysis of abrupt climate change between southern and northern Qinling Mountains in the past 50 years. *J. Shaanxi Norm. Univ.* **2010**, *38*, 98–105. [CrossRef]

23. Li, F. *Spatial-Temporal Changes and the Causes of Extreme Precipitation Events to the North and South of Qinling Mountain during 1962~2011*; Northwest Normal University: Lanzhou, China, 2014. [CrossRef]

24. Zhang, S.H. Spatial and temporal variation of precipitation in Qinling Mountains in the last 50 years. *J. Shangluo Univ.* **2014**, *28*, 62–66. [CrossRef]

25. Zhang, L.W.; Yan, J.P.; Geng, H.J.; Cao, Y.J. The shifts of annual average temperature and precipitation belts in the south and north region of Qinling Mountains, Shaanxi province. *J Shaanxi Norm. Univ.* **2011**, *39*, 81–84. [CrossRef]

26. Gao, X. *Study on Climate Change Trend and Spatial Distribution Characteristics of Qinling-Daba Mountains in Recent 50 Years*; Northwest University: Xi'an, China, 2011; Available online: https://kns.cnki.net/kcms2/article/abstract?v=3uoqIhG8C475KOm_zrgu4 lQARvep2SAkhskYGsHyiXksOA0FurgRFfHae_iXgbL9XHTnulT3WpybW6AjUBv9dOj-Y2ZAJvPY&uniplatform=NZKPT (accessed on 1 September 2021).

27. Song, T.X.; Yan, J.P.; Ma, L. Study on Climatic Differentiation in the South and North Qinling Mountains in Recent 50 Years. *Arid. Zone Res.* **2011**, *28*, 492–498. [CrossRef]

28. Zhang, Y.; Bai, H.Y.; Huang, X.Y.; Su, K. Variation of extreme temperature and its impact on regional warming in Qinling Mountains during recent 55 a. *Mt. Res.* **2018**, *36*, 23–33. [CrossRef]

29. Zhai, D.P.; Bai, H.Y.; Qin, J.; Deng, C.H.; Liu, R.J.; He, H. Temporal and spatial variability of air temperature lapse rates in Mt. Taibai, Central Qinling Mountains. *Acta Geogr. Sin.* **2016**, *71*, 1587–1595. [CrossRef]

30. Wang, T.; Yang, M.H.; Yan, S.J.; Geng, G.P.; Li, Q.H.; Wang, F. Effects of temperature and precipitation on spatiotemporal variations of net primary productivity in the Qinling Mountains, China. *Pol. J. Environ. Stud.* **2021**, *30*, 409–422. [CrossRef]

31. Wang, T. Analysis of the influence factors of topography on regional precipitation supported by GIS- A case study of Tianshui City, Gansu Province. *Gansu Sci. Technol.* **2012**, *28*, 58–61. [CrossRef]

32. Mann, H.B. Nonparametric tests against trend. *Econometrica* **1945**, *13*, 245–259. [CrossRef]

33. Kendall, M.G. Rank correlation methods. *Br. J. Psychol.* **1990**, *25*, 86–91. [CrossRef]

34. Du, R.S.; Shang, F.H.; Ma, N. Automatic mutation feature identification from well logging curves based on sliding *t* test algorithm. *Clust Comput.* **2019**, *22* (Suppl. 6), 14193–14200. [CrossRef]

35. Dogan, M.; Ulke, A.; Cigizoglu, H.K. Trend direction changes of Turkish temperature series in the first half of 1990s. *Theor. Appl. Climatol.* **2015**, *121*, 23–39. [CrossRef]

36. Zhang, Q.; Liu, C.L.; Xu, C.Y. Observed trends of annual maximum water level and streamflow during past 130 years in the Yangtze River basin, China. *J. Hydrol.* **2006**, *324*, 255–265. [CrossRef]

37. Song, X.Y.; Song, S.B.; Sun, W.Y. Recent changes in extreme precipitation and drought over the Songhua River Basin, China, during 1960–2013. *Atmos. Res.* **2015**, *157*, 137–152. [CrossRef]

38. Wei, F.F. *Modern Climate Statistical Diagnosis and Prediction Techniques*; China Meteorological Press: Beijing, China, 2007; ISBN 9787502942991.

39. Matheron, G. Principles of geostatistics. *Econ. Geol.* **1963**, *58*, 1246–1266. [CrossRef]

40. Zhang, J.; Yu, X.L. Analysis of land use change and its influence on runoff in the Puhe River Basin. *Environ. Sci. Pollut. Res.* **2021**, *28*, 40116–40125. [CrossRef]

41. Tang, G.A.; Yang, X. *Experimental Course of Spatial Analysis of Geographic Information System*; Science Press: Beijing, China, 2006; ISBN 9787030338969.

42. Olivwe, M.A.; Webster, R. Kriging: A method of interpolation for geographical information systems. *Int. J. Geogr. Inf. Sci.* **1990**, *4*, 313–332. [CrossRef]

43. Shi, Z.; Jin, H.M.; Li, Y.; Li, H.Y. Development and Application of Soft Package for Geostatistics. *J. Soil Water Conserv.* **2005**, *19*, 170–173. [CrossRef]

44. Li, X.J.; Li, C.K.; Yin, Z.H. ArcGIS based kriging interpolation and its application. *Bull. Surv. Mapp.* **2013**, *9*, 87–90. Available online: http://tb.chinasmp.com/CN/Y2013/V0/I9/87 (accessed on 1 September 2021).

45. Kang, L.W. *Spatial and Temporal Distribution of Rainstorm and Risk Assessment of Rainstorm Disasters in North and South Qinling Mountains of Shaanxi Province*; Shaanxi Normal University: Xi'an, China, 2014; Available online: http://cdmd.cnki.com.cn/article/cdmd-10718-1014403027.htm (accessed on 1 September 2021).

46. Pan, G.Y.; Cao, X.Y.; Zhang, X.; Tao, S.Y. Spatial and temporal characteristics of extreme precipitation in Ganjiang River Basin in the past 50 years. *Torrential Rain Disasters* **2020**, *39*, 102–108. [CrossRef]

47. Tang, T.; Jin, R.H.; Peng, X.Y.; Niu, R.Y. The Analysis of Causes about Extremely High Temperature in the summer of 2013 Year in the Southern Region. *J. Chengdu Univ. Inf. Technol.* **2014**, *29*, 652–659. [CrossRef]

48. Yan, J.P.; Huang, C.C. Statistical analysis on influence of ENSO event on the climate in Shaanxi. *J. Catastrophology* **1998**, *4*, 39–42.

49. Liu, M.X. *The Characteristics and Atmospheric Circulation Causes of Two Types of Extreme Cold Events in China*; Lanzhou University: Lanzhou, China, 2021. [CrossRef]

50. Li, D.; Gu, W. Analysis of characteristics and causes of precipitation anomalies over northern China in autumn 2021. *Meteor Mon.* **2022**, *48*, 494–503. (In Chinese) [CrossRef]

51. Hou, M.Q.; Fang, J.G.; Bai, A.J. Analysis of the weather and circulation characteristics of high temperature and drought in summer of 1997. *J. Shaanxi Meteorol.* **1999**, *1*, 4–7. Available online: http://www.cnki.com.cn/Article/CJFDTotal-SXQI901.001.htm (accessed on 1 September 2021).

52. Meng, Q.; Gao, X.; Bai, H.Y.; Zhang, Y.; Wang, H.Y. Temporal and spatial varirtions and trends of extreme precipitation in Qinling Mountains during the period 1960-2015. *Res. Soc. Water Conserv.* **2019**, *26*, 171–183. [CrossRef]

53. Du, J.Y.; Tao, L.; Xu, C.Y. Interdecadal variation of land precipitation in China and relative contributions of global warming, IPO and AMO. *Acta Meteorol. Sin.* **2022**, *80*, 685–700. [CrossRef]

54. Zhao, P.; Zhu, Y.N.; Zhang, R.H. An Asian-Pacific teleconnection in summer tropospheric temperature and associated Asian climate variability. *Clim Dynam.* **2007**, *29*, 293–303. [CrossRef]

55. Qi, Y.D. *Analysis of Temperature Change Trend and Its Urbanization and Sea-Atmosphere Impact Factors*; Wuhan University: Wuhan, China, 2020. [CrossRef]

56. Li, S.; Wang, Y.M.; Gao, Y.Q. A review of researches on the Atlantic Multidecadal Oscillation (AMO). *Trans. Atmos. Sci.* **2009**, *32*, 458–465. [CrossRef]

57. Zuo, Z.Y.; Zhang, R.H.; Wu, B.Y. Interdecadal variation of spring precipitation over southern China and its association with snow cover over Eurasia from 1979 to 2004. *Sci. Sin.* **2011**, *41*, 134–142. [CrossRef]

58. Zhao, H.Y.; Yang, Y.F.; Guo, J.Q.; Wang, X.; Zhao, Q.Y. Effect of Abnormal East Asia North Wind on Spring Precipitation in the Eastern Region of Northwest China. *Arid. Zone Res.* **2013**, *30*, 457–461. [CrossRef]

59. Gu, W.; Li Wj Chen, L.J.; Jia, X.L. Interannual variations of autumn precipitation in China and their relations to the distribution of tropical Pacific sea surface temperature. *Clim. Environ. Res.* **2011**, *17*, 467–480. [CrossRef]

60. Yang, J.H.; Zhang, Q.; Liu, X.Y.; Yue, P.; Shang, J.L.; Ling, H.; Li, W.J. Spatial-temporal characteristics and causes of summer precipitation anomalies in the transitional zone of typical summer monsoon, China. *Chin. J. Geophys.* **2019**, *62*, 4120–4128. [CrossRef]

61. Mu, X.M.; Chen, G.L.; Xu, X.X. Analysis on the relationship between precipitation and geographical factors in Loess Plateau. *Res. Soil Water Conserv.* **1992**, *16*, 80–86. Available online: http://stbcyj.paperonce.org/oa/DArticle.aspx?type=view&id=19920210 (accessed on 1 June 2022).

62. Li, C.; Zhang, H.; Singh, V.P.; Fan, J.; Wei, X.; Yang, J.T.; Wei, X.C. Investigating variations of precipitation concentration in the transitional zone between Qinling Mountains and Loess Plateau in China: Implications for regional impacts of AO and WPSH. *PLoS ONE* **2020**, *15*, e0238709. [CrossRef] [PubMed]

63. Li, S.S.; Lu, J.Y.; Yan, J.P.; Liu, X.F.; Kong, F.; Wang, J. Spatiotemporal variability of temperature in northern and southern Qinling Mountains and its influence on climatic boundary. *Acta Geogr. Sin.* **2018**, *73*, 13–24. [CrossRef]

64. Dong, D.H.; Huang, G. Relationship between Altitude and Variation Characteristics of the Maximum Temperature, Minimum Temperature, and Diurnal Temperature Range in China. *Chin. J. Atmos. Sci.* **2015**, *39*, 1011–1024. [CrossRef]

65. Schulze, H.; Langenberg, H. Climate science: Urban heat. *Nat. Geosci.* **2014**, *7*, 553. [CrossRef]

66. Dong, Q.Q.; Wang, H.X. Variation and reason analysis of temperature and precipitation of Weihe River in Guanzhong area in the last 60 years. *South–North Water Transf. Water Sci. Technol.* **2016**, *14*, 33–38. [CrossRef]

67. Li, M.J. *Analysis of Multi-Scale Spatial-Temporal Variability of Precipitation and Causes of Regional Drought and Flood in China*; University of Chinese Academy of Sciences: Beijing, China, 2021; Available online: https://d.wanfangdata.com.cn/thesis/Y3864553 (accessed on 1 June 2022).

68. Qiu, Y.H. *A Dissertation Submitted in Partial Fulfillment of The Requirements for the Degree of Master of Science*; Nanjing Normal University: Nanjing, China, 2019; Available online: https://mall.cnki.net/magazine/Article/CMFD/1019250006.htm (accessed on 1 June 2022).

69. Huang, M.D.; Zhang, P. Influences of geographic and topographic factors on spatial distribution of precipitation in Urumchi. *Meteorol. Sci. Technol.* **2009**, *37*, 25–28. [CrossRef]

70. Bi, X. *Analysis on Climate Change Characteristics of Temperature and Precipitation and the Correlation Analysis with Geographical Factors in Hubei Province*; Central China Normal University: Wuhan, China, 2013. [CrossRef]

71. Wang, P.; Tang, G.; Cao, L.; Liu, Q.; Ren, Y. Surface air temperature variability and its relationship with altitude & latitude over the Tibetan Plateau in 1981–2010. *Adv. Clim. Change Res.* **2012**, *8*, 313–319. [CrossRef]

72. Huang, X.C.; Wang, X.F.; Kang, L.W.; Wang, S. Temporal and spatial distribution characters of torrential rain in Qinling Area of Shaanxi Province. *Acta Agric. Jiangxi.* **2016**, *28*, 103–108. [CrossRef]

73. Su, J.Z.; Wen, M.; Ding, Y.H.; Gao, Y.Q.; Song, Y.F. Hiatus of global warming: A review. *Chin. J. Atmos. Sci.* **2016**, *40*, 1143–1153. [CrossRef]